THE JOURNAL OF PHYSICAL CHEMISTRY Letters

Letter

pubs.acs.org/JPCL

Molecular-Switch-Mediated Multiphoton Fluorescence Microscopy with High-Order Nonlinearity

Xinxin Zhu, Ya-Ting Kao, and Wei Min*

Department of Chemistry, Columbia University, New York, New York 10027, United States

ABSTRACT: Two-photon excited fluorescence microscopy is now an indispensable imaging tool for studying biological samples because of its intrinsic optical sectioning. However, both of its contrast and penetration depth are still limited when imaging deep inside of scattering samples. Herein, we propose a general spectroscopy concept to enhance the image contrast and the fundamental depth limit of two-photon imaging. We show that the population transfer kinetics of the photoinduced molecular switches could generate additional high-order nonlinearity between the signal and the laser intensity. Due to the long-lived nature of these switchable states, the incident photons can operate in a sequential manner, and the nonlinearity effect could accumulate (up to sixth order) as the population is being cycled through these states. Conceptually different from conventional multiphoton processes mediated by transient virtual states, our strategy constitutes a new class of fluorescence microscopy with high-order nonlinearity that is mediated by population transfer.

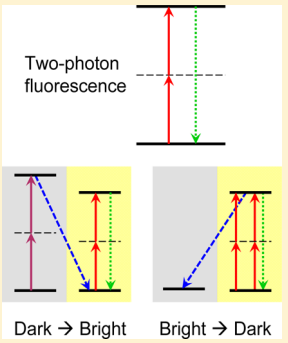

SECTION: Biophysical Chemistry and Biomolecules

Advances in optical imaging techniques have transformed the way that modern life sciences are conducted.[1,2] Among the current modalities, two-photon microscopy is the most popular for imaging highly scattering samples in vivo because even multiply scattered fluorescence photons can be assigned to their origin as the result of localized nonlinear signal generation.[3,4] Two-photon microscopy thus allows cellular imaging several hundred micrometers deep in various organs of living animals,[5,6] which constitutes a 3−5 fold increase in penetration depth when compared with confocal microscopy. However, its performance is still constrained by a fundamental imaging depth limit, which is determined by the obtainable contrast between the in-focus signal and the out-of-focus background.[7−11] Such a fundamental depth limit is formally defined as[7−11]

$$\left(\frac{S}{B}\right)_{\text{regular}} = \frac{\int_{V_{\text{in}}}\int_0^{\tau} C_S(r,z)I^2(r,z,t)\,\mathrm{d}t\,\mathrm{d}V}{\int_{V_{\text{out}}}\int_0^{\tau} C_B(r,z)I^2(r,z,t)\,\mathrm{d}t\,\mathrm{d}V} = 1 \quad (1)$$

where V_{in} is the focal volume, V_{out} is the sample volume but excluding the focal volume, r is the distance from the optical axis, z is the axial distance from the surface, C is the fluorophore concentration, I is the intensity of the two-photon imaging laser, and τ is the pixel dwell time. For mouse brain tissues labeled with GFP, the corresponding depth limit is about 1 mm.[8] Although this depth is impressive compared with that from other techniques, it still covers only a fraction of the mammalian brain. Obviously, this fundamental depth limit cannot be overcome by increasing laser power, which would enhance signal and background equally.

The quadratic dependence of the absorption rate on the incident laser intensity is the underlying principle for two-photon microscopy to exhibit spatially localized excitation. Because the limited imaging depth is a consequence of losing contrast between signal and background, it is reasonable to explore higher-order nonlinearity, which should exhibit a stronger discrimination against the background. In principle, this can be done by detecting three- or four-photon excited fluorescence. However, this seemingly viable approach is not practically attractive because (1) the simultaneous three- or four-photon absorption is an extremely improbable event whose amplitude is determined by the fifth- or seventh-order nonlinear polarizability, and (2) the excitation wavelength for GFP, YFP, and RFP needs to be between 1400 and 2200 nm, which lies outside of the transparent optical window of most biological tissues.[12]

In this Letter, we demonstrate that the unique dark−bright switching properties of special imaging probes could provide new sources of higher-order nonlinearity (up to sixth order) that could then enhance the signal-to-background ratio and effectively extend the fundamental imaging depth limit of two-photon microscopy. As depicted by energy diagrams in Figure 1, our new strategy harnesses new quantum states of special fluorophores to generate extra nonlinearity. This new approach does not require extremely high laser power or unfeasibly long wavelengths.

Transition from the Dark State to the Bright State. For fluorophores that can be switched from dark states to bright states, as shown in Figure 1B, we propose performing a multiphoton activation and imaging (MPAI) procedure in which the activation process from the dark state to the (bright) ground state is induced by a two-photon laser at a wavelength

Received: May 13, 2012
Accepted: July 18, 2012
Published: July 25, 2012

   dx.doi.org/10.1021/jz300607c | J. Phys. Chem. Lett. 2012, 3, 2082−2086

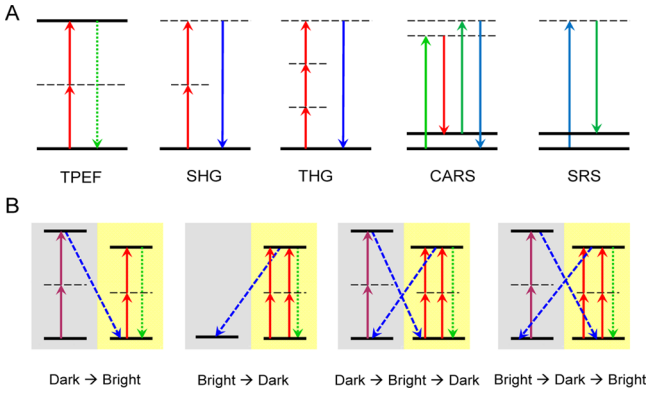

Figure 1. Energy diagrams of nonlinear optical processes. (A) Current nonlinear optical processes involve short-lived virtual states: TPEF (two-photon excited fluorescence); SHG (second-harmonic generation); THG (third-harmonic generation); CARS (coherent anti-Stokes Raman scattering); and SRS (stimulated Raman scattering). (B) Four distinct molecular-switch-mediated multiphoton fluorescence processes discussed in this study.

of λ_a with intensity of I_a and the subsequent imaging is excited by a laser at λ_i with intensity of I_i. After scanning by λ_a with a pixel dwell time of τ_a, $C(r,z)$ in eq 1 should be replaced by the concentration in the bright state, $A(r,z)$, which will scale with the activation yield, η, $A(r,z) = C(r,z)\eta(r,z,\tau_a)$. In the simplest condition, $\eta(t)$ follows a first-order chemical kinetics as $\eta(r,z,t) = 1 - \exp(-k_a t)$, where the rate constant k_a is proportional to the two-photon absorption cross section, σ_a, in units of Goppert–Mayer, $I_a^2(r,z)$ of the two-photon activation laser, its pulse width, δ, and its repetition rate, f_{rep}, and the quantum yield of dark-to-bright switching, φ_{DB}.

$$k_a = \sigma_a \delta f_{rep} \varphi_{DB} [I_a(r, z)\lambda_a/hc]^2 \quad (2)$$

The fluorescence signal of the final MPAI image of the activated bright state would then be

$$S_{MPAI} \propto (1 - e^{-k_a \tau_a}) I_i^2(r, z) C(r, z) \quad (3)$$

Transition from the Bright State to the Dark State. For fluorophores that can be switched from bright states to dark states under the same imaging laser wavelength λ_i, we can carry out a multiphoton deactivation and imaging (MPDI) procedure as shown in Figure 1B, taking a differential image before and after switching off of the bright states preferentially within the focus volume. The *pre*-deactivation image would be the same as that obtained with regular fluorophores. In contrast, the *post*-deactivation image will depend on the two-photon deactivation kinetics. When the switch is being illuminated by λ_i for a pixel dwell time of τ_d in a deactivation scanning, $C(r,z)$ in eq 1 would decrease with time. Following a first-order kinetics, the survival population $C(r,z,t) = C(r,z,t_0)e^{-k_d t}$ during $0 \le t \le \tau_d$ would have a deactivation rate constant of

$$k_d = \sigma_i \delta f_{rep} \varphi_{BD} [I_i(r, z)\lambda_i/hc]^2 \quad (4)$$

that is proportional to the two-photon absorption cross section at λ_i and the quantum yield of bright-to-dark switching, φ_{BD}. The final fluorescence signal in the differential image between the pre- and post-deactivation would be proportional to the deactivated population

$$S_{MPDI} \propto (1 - e^{-k_d \tau_d}) I_i^2(r, z) C(r, z, t_0) \quad (5)$$

Note that this result is analogous to that of the dark-to-bright transition in eq 3.

Cyclic Transitions between the Dark State and the Bright State. We now introduce two more complex scenarios (Figure 1B) in which the molecular switches undergo cyclic transition between dark states and bright states. Reversible switches will be needed here. For one scenario, the molecules start the cyclic transition from the dark state. Then, MPAI brings them to the bright state, resulting in a fluorescence signal as in eq 3. After that, we can go on to switch the activated bright population back to the dark state by a prolonged deactivation. Essentially, the final image of the MPAI will serve as the pre-deactivation image of MPDI. The resulting signal in this joint MPAI–MPDI procedure of dark–bright–dark transition would be

$$S_{cyclic} \propto (1 - e^{-k_a \tau_a})(1 - e^{-k_d \tau_d}) I_i^2(r, z) C(r, z, t_0) \quad (6)$$

For another scenario, the molecules start from the bright state, then go to the dark state via MPDI, and finally go back to the bright state via MPAI. Obviously, the final signal of this joint MPDI–MPAI procedure would exhibit the same formula as in eq 6.

High-Order Nonlinearity Associated with MPAI and MPDI. Having arrived at similar signal expressions for MPAI and MPDI, we now discuss the associated nonlinearity in terms of the dependence on the incident laser intensity. In addition to the obvious second dependence on the imaging laser, the population kinetics would lead to additional nonlinearity. When the laser intensity is low and/or the activation/deactivation dwell time is short, $1 - \exp(-k_{a/d}\tau_{a/d}) \propto I_{a/i}^2(r,z)$, offering an extra nonlinearity on the second order. In contrast, when the laser intensity is sufficiently high and/or there is a long enough $\tau_{a/d}$, $1 - \exp(-k_{a/d}\tau_{a/d}) \approx 1$, giving an effective zeroth-order dependence. In the intermediate region, the effective order value would vary continuously between 0 and 2.

Quantitatively, as illustrated by Figure 2A, the total intensity-dependent nonlinearity order, Ψ, of MPAI and MPDI signals would be

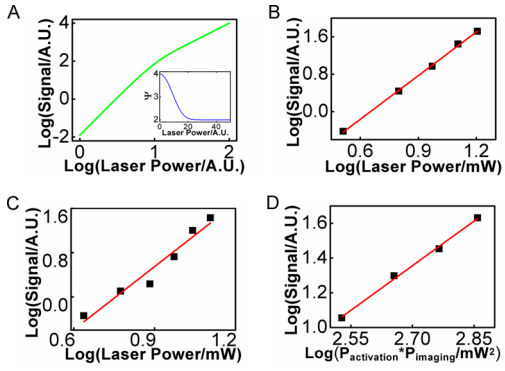

Figure 2. Nonlinear dependence of MPAI and MPDI signals on laser intensity. (A) The theoretical dependence of the signal on the laser intensity. The order of nonlinearity changes from fourth-order to second-order as the laser intensity increases. The experimental MPDI signal from Dronpa-3 (B) or Dronpa-1 (C) expressed *E. coli* cells shows a 3.1-order (B) or 3.8-order (C) nonlinear power dependence on the applied range of the 920 nm laser power. (D) The experimental MPAI fluorescence signal from PA-GFP expressing *E. coli* cells shows a 3.4-order nonlinear power dependence on the geometric mean of the 830 (for activation) and 920 nm (for imaging) laser powers.

dx.doi.org/10.1021/jz300607c | J. Phys. Chem. Lett. 2012, 3, 2082–2086

$$\Psi = \frac{2k_{a/d}\tau_{a/d}}{\exp(k_{a/d}\tau_{a/d}) - 1} + 2 \quad (7)$$

which is between 2 and 4. On the basis of similar analysis, the signal for cyclic transitions described in eq 6 would display nonlinearity with an order value between 2 to 6. Conceptually different from the conventional virtual-state-based nonlinear processes such as SHG and CARS,[13−16] the molecular-switching-based nonlinear effects described by eqs 3, 5, and 6 are created by population transfer kinetics between long-lived states in a sequential manner.

Better Contrast Originating from Higher-Order Nonlinearity. We can now analyze S/B for MPAI and MPDI images. On the basis of eqs 1, 3, and 5, we can express S/B of final images as

$$\left(\frac{S}{B}\right)_{MPAI/MPDI} = \frac{\int_{V_{in}}\int_0^{\tau} C_S(r,z)(1 - e^{-k_{a/d}\tau_{a/d}})I_i^2(r,z,t)\,dt\,dV}{\int_{V_{out}}\int_0^{\tau} C_B(r,z)(1 - e^{-k_{a/d}\tau_{a/d}})I_i^2(r,z,t)\,dt\,dV} \quad (8)$$

To quantify the above S/B, we need to analyze how the laser intensity is distributed within the scattering sample when the depth limit is reached for regular fluorophores as defined in eq 1. The fluorophores are often distributed throughout the 3D sample such as transgenic animal tissues with extensive FP expression. Thus, the number of out-of-focus fluorophores in the ground state is almost always orders-of-magnitude larger than that of the in-focus ones.

$$\frac{\int_{V_{in}} C_S(r,z)\,dV}{\int_{V_{out}} C_B(r,z)\,dV} \ll 1 \quad (9)$$

Therefore, when the depth limit is reached in eq 1, the excitation beam $I^2(r,z)$ at the focus will have to be much more intense than the out-of-focus counterpart to result in a similar level of fluorescence despite the scattering loss experienced by the laser beam.

As discussed earlier, the overall intensity-dependent nonlinearity order (between 2 and 4) of the MPAI and MPDI signals is higher than that of the regular two-photon microscopy. Thus, when coupled with more intense $I^2(r,z)$ at the focus as the depth limit is reached in eq 1, the higher-order nonlinearity of MPAI and MPDI should exhibit a stronger discrimination against the out-of-focus background. Extra order of nonlinearity should obtain more localized spatial information, which is also supported by the insight that the population transfer should occur predominantly within the focal volume rather than in the background. Therefore, when imaging at the depth limit defined in eq 1, $(S/B)_{MPAI/MPDI}$ should be much higher than unity, improving image contrast and extending the achievable imaging depth of two-photon microscopy. We note that our new concept works within the limit of eq 9, which could eventually break down when the excitation beam profile becomes significantly distorted in deep tissues.

Experimental Demonstration Using Optical Highlighter Fluorescent Proteins. Optical highlighters are an emerging family of fluorescent proteins that could change their states upon light illumination, either from the initial dark state into the bright state, switching between a bright state and a dark state, or converting from one color to another color.[17−21] Photoactivatable GFP (PA-GFP) stays originally in the dark state and must first be activated by 405 nm to be converted to the bright state, which is then readily excited to emit green fluorescence. PA-GFP expressed *E. coli* cells are densely dispersed in 2% agarose gel chunk to make a high-scattering tissue phantom. *E. coli* cells expressing regular GFP are used as a reference, and they are packed in the agarose gel with the same density based on the OD_{600} value. As shown in Figure 3A, the two-photon

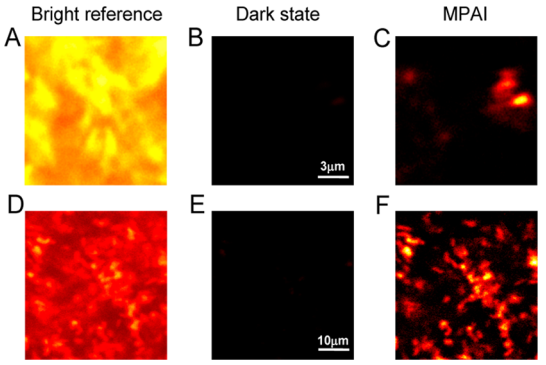

Figure 3. Demonstration of dark-to-bright state transition. (A) The image of densely packed 3D *E. coli* cells expressing normal GFP has an overwhelming background at a depth of 100 μm. (B) For 3D *E. coli* cells expressing PA-GFP, which have the same density as cells in (A), the preactivation image is almost dark at 100 μm. (C) After activation scanning by 830 nm, the subsequent MPAI image shows extremely high contrast. (D) For densely packed 3D *E. coli* expressing Dronpa-3, the preswitching image contrast is poor at a depth of 140 μm. (E) After a prolonged 488 nm illumination, which switched off Dronpa-3, the resulting image is almost dark. (F) The final MPAI image following an activation scanning by 800 nm reveals superior contrast to the original image of (D).

imaging of regular GFP shows an overwhelming out-of-focus background at a depth of 100 μm when excited at 920 nm, which is around the two-photon absorption peak of GFP.[22] In contrast, as shown in Figure 3B, PA-GFP expressed cells emit little fluorescence at 920 nm. In a MPAI experiment, after two-photon activation at 830 nm and then two-photon imaging at 920 nm, the final image in Figure 3C displays a much higher contrast at the same depth.

The bright-to-dark state transition is demonstrated with rsEGFP and Dronpa-3, which are two different photoswitchable FPs[23,24] that have been employed for many applications, including studying protein trafficking,[25] super-resolution microscopy,[26−29] removing autofluorescence,[30] photochromic FRET,[31] and recently as a genetically encoded viscosity reporter.[32] Irradiating rsEGFP and Dronpa-3 at 488 nm will generate green fluorescence. However, prolonged 488 nm illumination converts them to a dark state, and irradiation at 405 nm efficiently recovers the original bright state. As in PA-GFP, rsEGFP or Dronpa-3 expressed *E. coli* cells are densely dispersed to make high-scattering samples. In Figure 4A, the background is so high that the preswitching image of rsEGFP cells excited at 920 nm shows very poor contrast at a depth of 250 μm. After deactivating rsEGFP by a slow scanning at 920 nm, the postswitching image becomes a dimer in Figure 4B. The differential MPDI image in Figure 4C has a much higher S/B after normalization. Similar contrast enhancement is observed in Dronpa-3 expressed *E. coli* cells, as shown in Figure 4D−F.

Dark-to-bright state transition can also be achieved by reversible switches such as Dronpa-3, as shown in Figure 3D−

dx.doi.org/10.1021/jz300607c | J. Phys. Chem. Lett. 2012, 3, 2082−2086

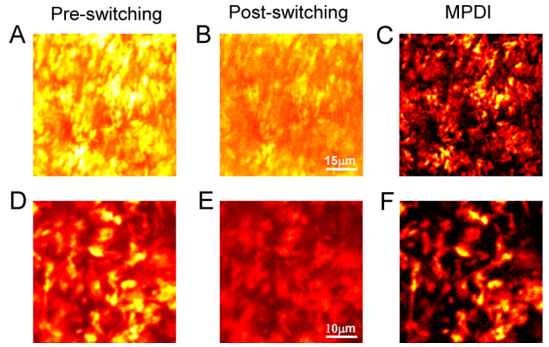

Figure 4. Demonstration of bright-to-dark state transition. (A) For densely packed 3D *E. coli* cells expressing rsEGFP, the regular preswitching image (excited at 920 nm) has an overwhelming background at a depth of 250 μm. (B) The postswitching image at the same condition as that of (A) shows a dimer signal. (C) The MPDI image (subtracting (B) from (A) and then autoscaling) offers an improved image contrast. (D) For densely packed 3D *E. coli* cells expressing Dronpa-3, the pre-switching image has a poor contrast at a depth of 250 μm. (E) After performing a slow deactivation scanning with 920 nm, the postswitching image is a dimer. (F) The MPDI image shows much improved contrast.

F. A brief 488 nm illumination efficiently switched Dronpa-3 in *E. coli* cells to the dark state in the sample volume. After that, two-photon activation by scanning with a 800 nm laser and subsequent imaging under 920 nm resulted in a remarkable image contrast of cells at the focal plane. Compared to MPAI with PA-GFP, MPAI using Dronpa-3 requires the extra switching-off step at the beginning but benefits from relatively more efficient activation due to the higher φ_{DB}. Hence, both proteins should find applications in biological tissues.

Finally, we verify the high-order nonlinear intensity dependence of both the MPAI signal (with PA-GFP) and the MPDI signal (with two Dronpa variants, Dronpa-3 and Dronpa-1). As shown in Figure 2B–D, nonlinearity orders are observed between 3.1 and 3.8 for the corresponding optical highlight proteins inside of *E. coli* cells with the experimentally applied laser intensities and pixel dwell times of activation (for MPAI) or deactivation (for MPDI). These measured values of nonlinearity orders are consistent with the theoretical prediction (eq 7) of an overall nonlinearity order between 2 to 4.

In this study, we have theoretically and experimentally demonstrated molecular-switch-mediated nonlinearity for two-photon fluorescence microscopy. Most notably, its high-order nonlinearity is rooted in the population transfer kinetics from or into the real states, which is profoundly distinct from the conventional multiphoton microscopy whose nonlinearity stems from the (almost) simultaneous interaction of incident photons via transiently lived virtual states.[13−16] Due to the long-lived nature of the molecular switches, the incident photons can operate temporally, and the nonlinearity effect can accumulate up to sixth-order as the population cycles between these states. On the basis of the generated higher-order nonlinearity, we obtained more localized spatial information with superior image contrast than the regular two-photon microscopy. The present strategy toward imaging the depth limit is reminiscent of super-resolution microscopy techniques that also harness the switching capability of imaging probes.[33−36]

EXPERIMENTAL SECTION

Imaging. All of the two-photon fluorescence images were taken on a Leica TCS SP5 MP inverted microscope equipped with a Mai Tai HP laser (690−1040 nm) and an HCX PL APO CS 20X DRY microscope objective (N.A. = 0.70). A nondescanned epi PMT placed directly behind the objective was used for fluorescence collection in combination with a 680SP emission filter. Data in Figure 2 were taken under a pixel dwell time of 65 μs. Images of *E. coli* expressing regular GFP (Figure 3A) were taken under 920 nm (64mW) with a pixel dwell time of 20 μs. Images of pa-GFP *E. coli* (Figure 3B, C) were taken under 920 nm (64mW) with a dwell time of 200 μs after four frames of two-photon activation under 830 nm (95mW) with a dwell time of 200 μs (Figure 3C). Images of Dronpa-3 *E. coli* (Figure 3D−F) were taken under 920 nm (99 mW) with a pixel dwell time of 40 μs. An activation scanning at 800 nm (2.9 mW) with a pixel dwell time of 80 μs was performed prior to the subsequent imaging of Figure 3F. Images of rsEGFP *E. coli.* (Figure 4A,B) were taken under 920 nm (83mW) with a pixel dwell time of 40 μs. Images of Dronpa-3 *E. coli.* (Figure 4D,E) were taken under 920 nm (99 mW) with a dwell time of 40 μs, between which a slow deactivation scanning at 920 nm (99 mW) with a dwell time 160 μs was performed. Note that due to the strong scattering of the prepared tissue phantoms, the actual laser power reached at the focus is lower than the measured power transmitted through the objective. All images are with 512 × 512 pixels.

Sample Preparation. In live bacteria-imaging experiments presented in Figures 2−4, PA-GFP (Addgene plasmid 11911) and rsEGFP (Abberior) were expressed in BL21 *E. coli* strains, and Dronpa-3 and Dronpa-1 expressing *E. coli* cells were prepared as previously reported[32] and then harvested by centrifugation, resuspended, and embedded inside of an imaging spacer using 2% agarose gel. The imaging spacer (Sigma S7935) was pasted between two pieces of micro-coverglass (VWR 48393-220). *E. coli* densities of different samples were calibrated based on the OD_{600} measurement to achieve a consistent scattering effect.

AUTHOR INFORMATION

Corresponding Author

*E-mail: wm2256@columbia.edu.

Notes

The authors declare no competing financial interest.

ACKNOWLEDGMENTS

We thank Zhixing Chen, Lu Wei, Louis Brus, Rafael Yuste, Nicholas Turro, Virginia Cornish, and Darcy Peterka for helpful discussions. W.M. acknowledges the start up funds from Columbia University and grant support from Kavli Institute for Brain Science.

REFERENCES

(1) Pawley, J. B., Ed. *Handbook of Biological Confocal Microscopy*, 3rd ed.; Springer: New York, 2006.

(2) Yuste, R., Ed. *Imaging: A Laboratory Manual*; Cold Spring Harbor Press: Plainview, NY, 2010.

(3) Denk, W.; Strickler, J. H.; Webb, W. W. Two-Photon Laser Scanning Microscopy. *Science* **1990**, *352*, 73−76.

(4) Zipfel, W. R.; Williams, R. M.; Webb, W. W. Nonlinear Magic: Multiphoton Microscopy in the Biosciences. *Nat. Biotechnol.* **2003**, *21*, 1369−1377.

(5) Helmchen, F.; Denk, W. Deep Tissue Two-Photon Microscopy. *Nat. Methods* **2005**, *2*, 932−940.
(6) Masters, B. R.; So, P. T. C., Eds. *Handbook of Biomedical Nonlinear Optical Microscopy*; Oxford University Press: New York, 2008.
(7) Ying, J.; Liu, F.; Alfano, R. R. Spatial Distribution of Two-Photon-Excited Fluorescence in Scattering Media. *Appl. Opt.* **1999**, *38*, 224−229.
(8) Theer, P.; Hasan, M. T.; Denk, W. Two-Photon Imaging to a Depth of 1000 Micro in Living Brains by use of a Ti:Al_2O_3 Regenerative Amplifier. *Opt. Lett.* **2003**, *28*, 1022−1024.
(9) Theer, P.; Denk, W. On the Fundamental Imaging-Depth Limit in Two-Photon Microscopy. *J. Opt. Soc. Am. A* **2006**, *23*, 3139−3149.
(10) Kobat, D.; Horton, N. G.; Xu, C. In Vivo Two-Photon Microscopy to 1.6-mm Depth in Mouse Cortex. *J. Biomed. Opt.* **2011**, *16*, 106014.
(11) Durr, N. J.; Weisspfennig, C. T.; Holfeld, B. A.; Ben-Yakar, A. Maximum Imaging Depth of Two-Photon Autofluorescence Microscopy in Epithelial Tissues. *J. Biomed. Opt.* **2011**, *16*, 026008.
(12) Wang, P.; Wang, H.-W.; Sturek, M.; Cheng, J.-X. Bond-Selective Imaging of Deep Tissue through the Topical Window between 1600 and 1850 nm. *J. Biophotonics* **2012**, *5*, 25.
(13) Levenson, M. D.; Kano, S. S. *Introduction to Nonlinear Laser Spectroscopy*; Academic Press: San Diego, CA, 1988.
(14) Shen, Y. R. *The Principles of Nonlinear Optics*; Wiley: New York, 1984.
(15) Warren, W. S.; Fischer, M. C.; Ye, T. Novel Nonlinear Contrast Improves Deep-Tissue Microscopy. *Laser Focus World* **2007**, *43*, 99−103.
(16) Min, W.; Freudiger, C. W.; Lu, S.; Xie, X. S. Coherent Nonlinear Optical Imaging: Beyond Fluorescence Microscopy. *Annu. Rev. Phys. Chem.* **2011**, *62*, 507−530.
(17) Lippincott-Schwartz, J.; Patterson, G. H. Photoactivatable Fluorescent Proteins for Diffraction-Limited and Super-Resolution Imaging. *Trends in Cell Biology* **2009**, *19*, 555−565.
(18) Chudakov, D. M.; Matz, M. V.; Lukyanov, S.; Lukyanov, K. A. Fluorescent Proteins and their Applications in Imaging Living Cells and Tissues. *Physiol Rev.* **2010**, *90*, 1103−1163.
(19) Wu, B.; Piatkevich, K. D.; Lionnet, T.; Singer, R. H.; Verkhusha, V. V. Modern Fluorescent Proteins and Imaging Technologies to Study Gene Expression, Nuclear Localization, and Dynamics. *Curr. Opin. Cell Biol.* **2011**, *23*, 310−317.
(20) Heilemann, M.; Dedecker, P.; Hofkens, J.; Sauer, M. Photoswitches: Key Molecules for Subdiffraction-Resolution Fluorescence Imaging and Molecular Quantification. *Laser Photonics Rev.* **2009**, *3*, 180−202.
(21) Patterson, G. H. Highlights of the Optical Highlighter Fluorescent Proteins. *J. Microsc.* **2011**, *243*, 1−7.
(22) Schneider, M.; Barozzi, S.; Testa, I.; Faretta, M.; Diaspro, A. Two-Photon Activation and Excitation Properties of PA-GFP in the 720−920-nm Region. *Biophys. J.* **2005**, *89*, 1346−1352.
(23) Ando, R.; Flors, C.; Mizuno, H.; Hofkens, J.; Miyawaki, A. Highlighted Generation of Fluorescence Signals using Simultaneous Two-Color Irradiation on Dronpa Mutants. *Biophys. J.* **2007**, *92*, L97−L99.
(24) Grotjohann, T.; Testa, I.; Leutenegger, M.; Bock, H.; Urban, N. T.; Lavoie-Cardinal, F.; Willig, K. I.; Eggeling, C.; Jakobs, S.; Hell, S. W. Diffraction-Unlimited All-Optical Imaging and Writing with a Photochromic GFP. *Nature* **2011**, *478*, 204−208.
(25) Ando, R.; Mizuno, H.; Miyawaki, A. Regulated Fast Nucleocytoplasmic Shuttling Observed by Reversible Protein Highlighting. *Science* **2004**, *306*, 1370−1373.
(26) Hofmann, M.; Eggeling, C.; Jakobs, S.; Hell, S. W. Breaking the Diffraction Barrier in Fluorescence Microscopy at Low Light Intensities by Using Reversibly Photoswitchable Proteins. *Proc. Natl. Acad. Sci. U.S.A.* **2005**, *102*, 17565−17569.
(27) Flors, C; et al. A Stroboscopic Approach for Fast Photoactivation-Localization Microscopy with Dronpa Mutants. *J. Am. Chem. Soc.* **2007**, *129*, 13970−13977.
(28) Andresen, M.; Stiel, A. C.; Fölling, J.; Wenzel, D.; Schönle, A.; Egner, A.; Eggeling, C.; Hell, S. W.; Jakobs, S. Photoswitchable Fluorescent Proteins Enable Monochromatic Multilabel Imaging and Dual Color Fluorescence Nanoscopy. *Nat. Biotechnol.* **2008**, *26*, 1035−1040.
(29) Rego, E. H.; Shao, L.; Macklin, J. J.; Winoto, L.; Johansson, G. A.; Kamps-Hughes, N.; Davidson, M. W.; Gustafsson, M. G. Nonlinear Structured-Illumination Microscopy with a Photoswitchable Protein Reveals Cellular Structures at 50-nm Resolution. *Proc. Natl. Acad. Sci. U.S.A.* **2012**, *109*, E135−143.
(30) Marriott, G.; Mao, S.; Sakata, T.; Jackson, D.; Gomez, T.; Aaron, H.; Isacoff, E. Y.; Yan, Y. High Contrast Imaging Based on Optical Lock-In Detection Imaging of Synthetic and Genetically Encoded Optical Switches. *Proc. Natl. Acad. Sci. U.S.A.* **2008**, *46*, 17789−17794.
(31) Mao, S.; Benninger, R. K.; Yan, Y.; Petchprayoon, C.; Jackson, D.; Easley, C. J.; Piston, D. W.; Marriott, G. Optical Lock-In Detection of FRET Using Synthetic and Genetically Encoded Optical Switches. *Biophys. J.* **2008**, *94*, 4515−4524.
(32) Kao, Y.-T.; Zhu, X.; Min, W. Protein Flexibility Mediated Coupling between Photoswitching Kinetics and the Surrounding Viscosity of a Photochromic Fluorescent Protein. *Proc. Natl. Acad. Sci. U.S.A.* **2012**, *109*, 3220−3225.
(33) Hell, S. W. Far-Field Optical Nanoscopy. *Science* **2007**, *316*, 1153−1158.
(34) Rust, M. J.; Bates, M.; Zhuang, X. Sub-Diffraction-Limit Imaging by Stochastic Optical Reconstruction Microscopy (STORM). *Nat. Methods* **2006**, *3*, 793−795.
(35) Betzig, E.; et al. Imaging Intracellular Fluorescent Proteins at Nanometer Resolution. *Science* **2006**, *313*, 1642−1645.
(36) Hess, S. T.; Girirajan, T. P. K.; Mason, M. D. Ultra-High Resolution Imaging by Fluorescence Photoactivation Localization Microscopy. *Biophys. J.* **2006**, *91*, 4258−4272.